Neutron scattering study of adsorption in porous MCM-41 silica[1]

R.J.C. Brown, M.J.B. Evans, and Z. Tun

Abstract: Adsorption of *n*-pentane on MCM-41 silica has been studied by neutron scattering on both the adsorption and desorption isotherms. Adsorption takes place without hysteresis in either the isotherm or the neutron scattering profile. Adsorption of contrast-matched pentane in porous MCM-41 silica at first increases the intensity of the (10) Bragg peak but reduces the (11) and (20) peaks, and as the pores are filled the intensities of all Bragg peaks are reduced to zero. The SANS background has a $1/Q$ dependence, typical of a material prepared with templates of one-dimensional character (cylinders). The initial increase of (10) intensity allows estimation of the cylindrical pore diameter to be 37 Å based on the variation of form factor as a function of the cylinder radius.

PACS Nos: 61.43.Gt, 61.46.Bc, 81.05.Rm, 82.75.Fq

Résumé : Nous avons étudié l'adsorption du *n*-pentane sur de la silice MCM-41 par diffusion de neutrons sur les deux isothermes d'adsorption et de désorption. L'adsorption se produit sans hystérèse soit dans l'isotherme ou le profil de diffusion de neutrons. Au début, l'adsorption en appariement de contraste du n-pentane dans la silice MCM-41 augmente l'intensité du pic (10) de Bragg, mais réduit celle des pics (11) et (20). À mesure que les pores se remplissent, l'intensité de tous les pics de Bragg diminue à zéro. Le bruit de fond de la diffusion de neutrons à petits angles (SANS) a une dépendance en $1/Q$ typique d'un matériau préparé avec des gabarits de type unidimensionnels (cylindres). L'augmentation initiale de l'intensité du pic (10) permet d'estimer que le diamètre des pores cylindriques est 37 Å en se basant sur la variation du facteur de forme en fonction du rayon du cylindre.

[Traduit par la Rédaction]

1. Introduction

The interaction between gases and porous solids is an important method for studying the nature of porosity. Although standard procedures are available for interpreting the shapes of the adsorption and desorption isotherms, there is ambiguity in the interpretation of the various types of isotherm. Similar isotherms can result from more than one arrangement of empty space within the solid, and deduction of the nature of porosity of a sample from the observed isotherm depends upon assumptions about the nature of the porosity and the distribution of the adsorbed fluid within the pores. Therefore, isotherms themselves are usually not enough information upon which to base firm conclusions, particularly in cases where percolation effects in a system of interconnected pores influence the desorption process [1–3].

Our objective in this experiment is to apply neutron scattering to determine how the distribution of adsorbate within a porous solid changes through the adsorption–desorption cycle in a simple mesoporous solid, MCM-41, whose nature of porosity is fairly well known. Absolute constancy of the factors that control diffracted intensity (volume of the MCM-41 powder and the orientation of the grains) was ensured in our experiment by keeping the sample absolutely stationary in the neutron beam during the entire adsorption–desorption cycle. This strategy of carrying out adsorption–desorption cycles in situ with neutron scattering has been employed by various researchers in the study of porous materials [4–8].

MCM-41 is a highly porous form of silica, formed by precipitating silica in the presence of surfactant micelles. The geometrical arrangement of pores is known from X-ray diffraction and electron microscopy to be a fairly well ordered hexagonal array of parallel cylindrical pores in which the spacing between the pores is about 41 Å [9]. The adsorbate chosen was *n*-pentane, isotopically contrast-matched to the host, as explained in detail in the next section. The pressure–temperature characteristic of pentane is such that its vapour pressure can be easily controlled at a temperature not far from room temperature. Moreover, the use of pentane, a molecule of different area coverage from N_2, gives an independent evaluation of the adsorption process.

2. Experimental

The MCM-41 powder sample was prepared by a standard method [10]. As final preparation for the adsorption experiments, the sample was calcined in air using a muffle furnace at a temperature of 813 K. X-ray diffraction (Cu K_α) gave

Received 19 June 2009. Accepted 31 August 2009. Published on the NRC Research Press Web site at cjp.nrc.ca on 24 March 2010.

R.J.C. Brown. Chemistry Department, Queen's University, Kingston, ON K7L 3N6, Canada.
M.J.B. Evans. Department of Chemistry and Chemical Engineering, Royal Military College, Kingston, ON K7K 7B4, Canada.
Z. Tun.[2] Canadian Neutron Beam Centre, National Research Council Canada, Chalk River, ON K0J 1J0, Canada.

[1]Special issue on Neutron Scattering in Canada.
[2]Corresponding author (e-mail: zin.tun@nrc.gc.ca).

Fig. 1. The N_2 adsorption (●) and desorption (○) isotherms at 77 K determined by the volumetric method. The amount adsorbed is shown as the volume of N_2 at STP normalized for 1 g of MCM-41 powder sample.

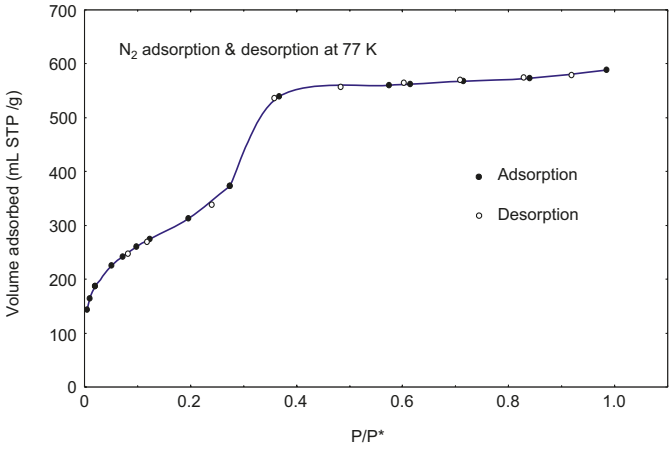

the expected powder pattern, from which the spacing between the centres of the cylindrical pores, a, was found to be 45 Å. Neutron diffraction on the same sample gave a = 44.2 Å, where the difference could be the result of slight misalignment of either the X-ray or neutron diffractometer or a small error in the neutron wavelength calibration. For consistency, we will adopt 44.2 Å as the cylindrical pore spacing throughout our analysis of neutron results and the ensuing discussion.

The sample was further characterized by measuring adsorption–desorption isotherm for N_2 at 77 K using a volumetric apparatus Micromeritics ASAP 2000. The resulting isotherm shown in Fig. 1 is of type IVc (ref. 1, p. 441) with no hysteresis. The five adsorption data points that lie within the range of P/P^* = 0.05 to 0.20 were used to determine the Brunauer–Emmett–Teller (BET) specific surface area (1160 ± 19 m^2/g). A pore size distribution analysis by the Barrett, Joyner, and Halenda (BJH) method [11] on the same isotherm gave a narrow distribution with an average pore diameter of 24 Å. Combining these results, the total pore length is of order 10^{11} m/g. The specific surface area calculated from the average pore diameter derived from the BJH analysis is 280 m^2/g, considerably smaller than the value based on the BET analysis.

Prior to neutron scattering experiments, the adsorption–desorption isotherm at 298.15 K with n-pentane of natural isotopic abundance as the adsorbate was also measured, using a gravimetric apparatus based on a helical quartz spring. The resulting isotherm is similar to Fig. 1, and applying the BET equation to the same pressure range, P/P^* = 0.05 to 0.20, yields the same specific surface area as do the N_2 data (within 1%) . In a separate experiment, the isotherm was determined by a volumetric method, yielding results that are in agreement with the gravimetric method.

For the neutron experiment, a portable vacuum rack was constructed, consisting of a reservoir for liquid pentane, a pressure transducer and a sample container connected to the reservoir by a flexible metal tube. The closed system allowed traversing of the adsorption–desorption cycle with pressure as the independent variable simply by setting the temperature of the thermostat-controlled bath in which the reservoir was immersed. This procedure is similar to that used by Hoinkis [6]. The reservoir temperature and pressure transducer readings were constantly monitored and logged throughout the experiment. The sample was thermostat controlled at 293.48 K, which was well below the ambient temperature to avoid condensation in the tubing.

For the purpose of contrast matching, which has the benefit of simplifying the analysis of neutron results, we prepared a mixture of n-pentane with isotopic ratio C_5H_{12}/C_5D_{12} = 41.6:58.4. The coherent scattering length density of the liquid is equal to SiO_2 of specific gravity 2.05, ~12% less dense than crystalline form of SiO_2 (cristobalite). The lower density accounts for the fact that the calcined SiO_2 skeleton is not a perfect crystalline phase but an amorphous material with defects and micropores. Provided our strategy of contrast matching is satisfactory, a thin layer of adsorbate on the surface of a pore will appear to the neutrons as a reduction in the pore radius, whereas a pore filled with liquid will cease contributing to coherent scattering.

Neutron scattering measurements were carried out at the NRU reactor, Chalk River, using the C5 spectrometer, and the spectrometer set-up (choice of monochromator, collimation, etc.) was similar to that described previously [12]. Being a spectrometer equipped with only a single detector (i.e., not a multipixel 2-dimensional detector commonly found on SANS instruments), each data collection "run" consists of scanning the detector over a range of Bragg angle 2θ. The neutron wavelength, λ, was 2.37 Å and the range of Q thus covered was from 0.040 to 0.410 $Å^{-1}$ for most runs. The magnitude of $\boldsymbol{Q}$ relates to the Bragg angle customarily as $4\pi\sin\theta/\lambda$.

Starting with a 480.6 mg sample in vacuo, the temperature of the pentane reservoir was increased in steps between collecting the neutron scattering data. The increase in temperature was carried out over a period of about 1 h, and the sample was left to equilibrate for at least an additional hour at constant pressure; with this procedure, there was never any overshoot in the amount of pentane adsorbed in the sample. The maximum pressure reached in the neutron experiment was P/P^* = 0.3209, which lies well above the pressure at which the pores are filled. The pentane reservoir temperatures (T) at which neutron data were taken are summarized in Table 1 along with the corresponding pressures (P). We stress here that the T values listed are only nominal, while our analysis is based entirely on the pressure (P) readings. The pressure P^* our partially deuterated pentane would have at the sample temperature is estimated from the results reported by Hörner et al. [13], showing C_5D_{12} to be more volatile than C_5H_{12}. Consequently, the deuteration level will be higher in the vapour phase (i.e., in the transfer tube). However, we expect the preferential evaporation of C_5D_{12} to reverse when the vapour condenses within the pores of the sample, leading to a deuteration similar to the liquid in the reservoir.

Intensity profiles obtained during absorption are shown in Fig. 2. Counts as recorded by the single-detector are plotted without corrections or modifications. Profiles were measured at the same pressure settings during the desorption part of the experiment as well but are not shown as they superimpose exactly with the results in Fig. 2 (i.e., within random fluctuations consistent with counting statistics). This recov-

Table 1. Chronological sequence of neutron diffraction scans identified by nominal reservoir temperatures, with either a prefix A (adsorption) or D (desorption). P^* = 60.043 kPa is the vapour pressure at 293.48 K for pentane with the C_5D_{12} molar fraction of 0.584 (estimate based on ref. 11). The fraction of mesopore volume filled is determined from the gravimetric isotherm of Fig. 4, adopting filling = 1 at P/P^* of 0.261. Listing of this quantity here amounts to assuming that the fractional filling for the mixture at 293.48 K is the same as that for natural isotopic pentane at 298.15 K.

Pentane reservoir temperature T (K)	Pressure P (kPa)	P/P^*	Fraction of mesopore volume filled
77 (liq N_2)	0	0.000	0.00
A239	4.265	0.0710	0.17
A253	9.565	0.1593	0.36
A258	12.454	0.2074	0.52
A261	14.511	0.2417	0.80
A264	16.864	0.2809	1.00
A267	19.270	0.3209	1.02
D264	16.891	0.2813	1.01
D261	14.560	0.2425	0.80
D258	12.497	0.2081	0.50
D253	9.582	0.1596	0.36
D240	4.297	0.0716	0.17
D77 (liq N_2)	0	0.000	0.00

Fig. 2. Neutron scattering profiles. The inset shows the in-vacuo profile plotted on a log-log scale along with an underlying straight line whose slope is –1. For greater clarity afforded by colour-coded curves, see the paper online by accessing the electronic version of Can. J. Phys.

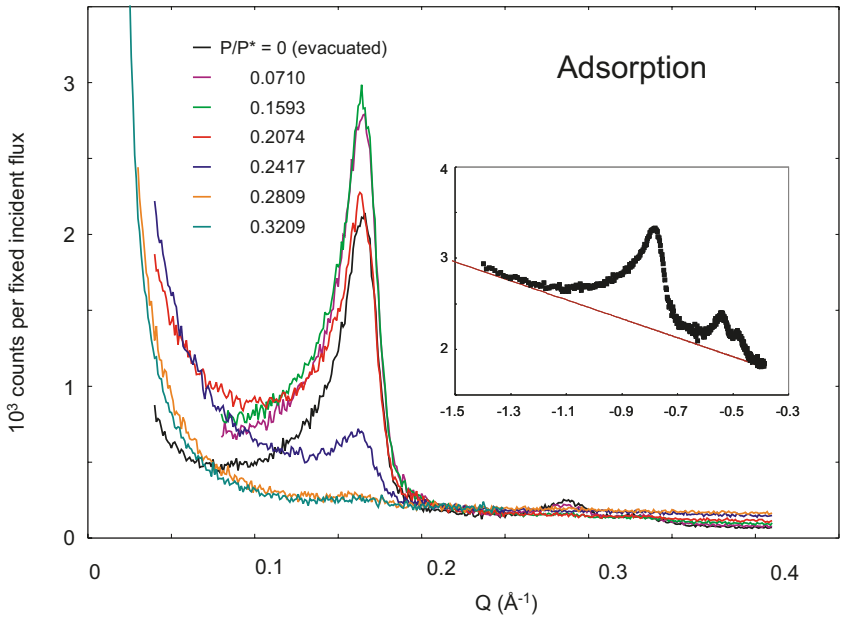

ery of the original diffraction profile shows that the calcined SiO_2 skeleton is not irreversibly affected by the pentane. The last run of the experiment was the pentane condensed in the reservoir at 77 K, and no residual pressure was observed in the system, indicating that the system had remained free of leaks for the 8-day duration of the experiment.

3. Results and discussion

The intensity profiles in Fig. 2 clearly show four distinct regions in the ascending order of Q:

(1) The SANS region at the lowest Q, up to $Q \sim 0.08$ Å^{-1}.
(2) The first-order diffraction peak from the mesopore structure, centred at Q = 0.164 Å^{-1} but with tails extending from $Q \sim 0.1$ to 0.2 Å^{-1}.
(3) The region of higher-order peaks that extends from $Q \sim 0.25$ to 0.35 Å^{-1}.
(4) The "high-Q" background at $Q > 0.36$ Å^{-1}.

The inset in Fig. 2 is a re-plot of the in-vacuo data on a log–log scale. The higher order peaks are more clearly visible in this plot. It also shows, by a straight line of slope –1, that there is an underlying $1/Q$ intensity variation over the entire scan.

Fig. 3. High-Q regions of the neutron scattering profiles. For greater clarity afforded by colour-coded curves, see the paper online by accessing the electronic version of Can. J. Phys.

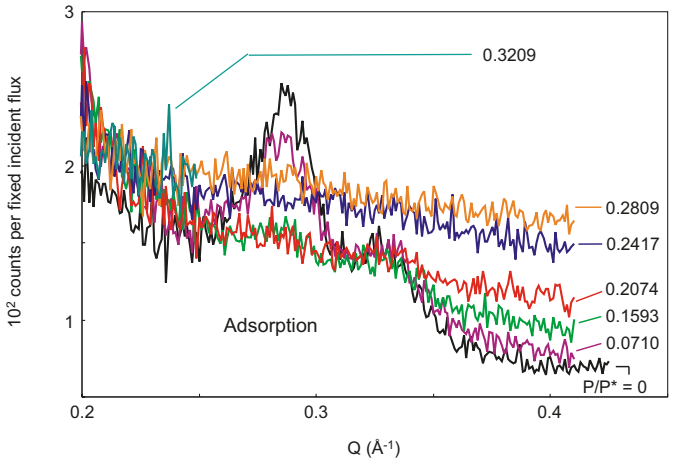

Fig. 4. The low-pressure portion of the gravimetric isotherm at 298.15 K with natural isotopic pentane as the adsorbate. Also plotted are the excess counts of neutrons beyond those scattered by the fully evacuated sample as partially deuterated pentane was adsorbed and subsequently desorbed. Expressed in P/P^*, it is expected that natural-isotopic and partially-deuterated pentane would achieve similar fractional filling of the pores.

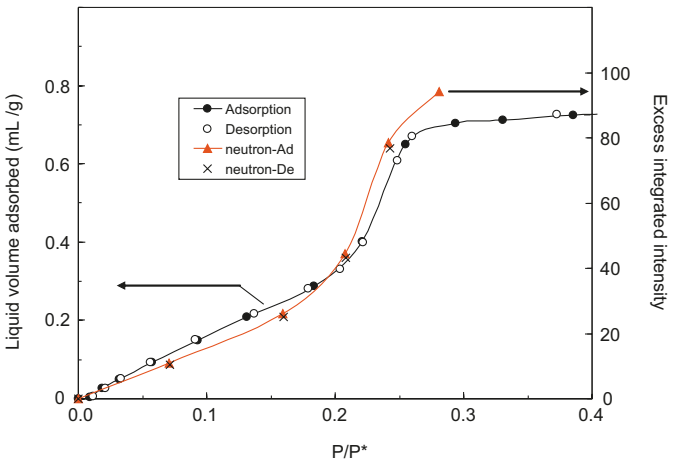

We will begin with a discussion on the behaviour of the high-Q background. For better clarity, neutron intensities with $Q > 0.2$ Å^{-1} are plotted again in Fig. 3 with expanded scales. The "high-Q" background monotonically increases during adsorption. This increase is mostly, if not entirely, due to the incoherent elastic scattering of hydrogen, and is therefore expected to be directly proportional to the amount of pentane absorbed in the sample. Had we made additional measurements using standards (e.g., known amount of a material with large incoherent elastic scattering cross-section such as vanadium), we would be able to normalize the intensity on an absolute scale and thus estimate the amount of pentane directly from this "background".

Figure 4 is our attempt to verify the above hypothesis: it shows the low pressure end of pentane adsorption–desorption (gravimetric) isotherm, superimposed with neutron counts that are in excess of the background observed with the fully evacuated sample. For better statistics in determining the excess counts, we included all the data with $Q > 0.36$ Å^{-1}. The figure shows that a reasonable agreement between neutron and gravimetric results can be achieved by adjusting the scale for the neutron counts, the right-hand y-axis in the figure, if we ignore the point at $P/P^* = 0.2809$. The good agreement over most of the pressure range confirms that the increase of high-Q background as pentane is adsorbed is largely due to incoherent scattering off the hydrogen. However, some other factor beyond this simple phenomenon came into action once the mesopores were filled at $P/P^* \sim 0.25$. It could be that the pentane adsorbed thereafter condensed somewhere outside the mesopores with a certain positional order so that a broad diffraction peak was developing at a Q beyond our scan range. Excess neutrons from the tail of that peak will then lead to an outlier in the otherwise good agreement.

Fig. 5. Square of the form factor, $|F_c(Q)|^2$, representing scattering intensity from cylinders of various diameters D.

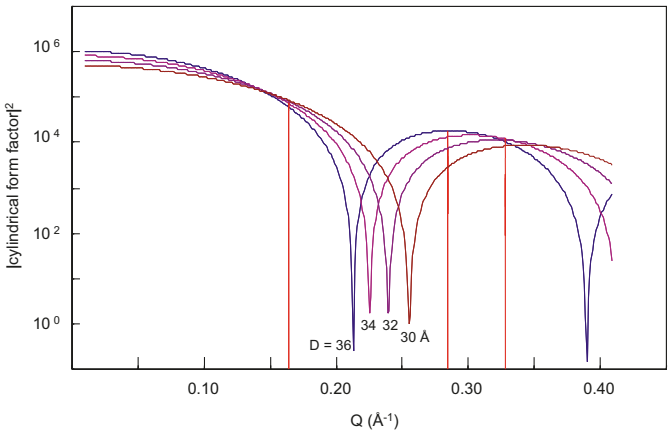

Fig. 6. Magnitude of the $|F_c(Q)|^2$ at the location of the first-order Bragg peak ($Q = 0.164$ Å^{-1}) as a function of D.

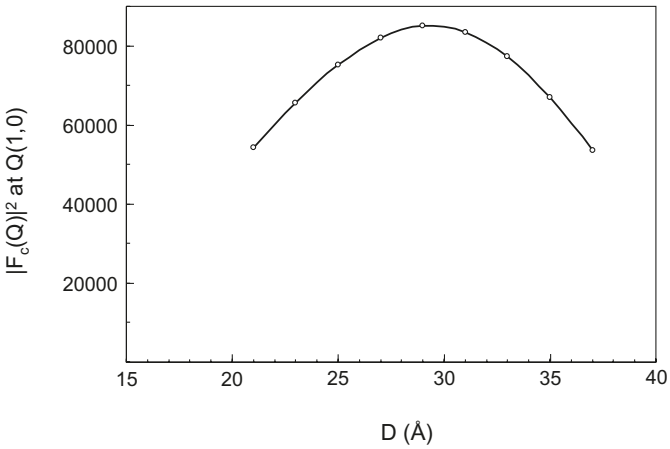

In the SANS region, the intensity initially increases as the pentane is adsorbed, but the change is not monotonic. The intensity becomes strongest around $P/P^* \sim 0.21$, and drops significantly at higher pressures. When the peaks from the mesopore structure became almost zero by complete contrast matching, the SANS intensity had greatly fallen, but it clearly remained above that of the in-vacuo scan. Qualitatively, we know that SANS arises from correlations over

large distances; distances larger than ~80 Å in this case, corresponding to $Q < 0.08$ Å^{-1}. The intensity increase is either because there are more of the regions with this characteristic size, or the variation of contrast over such a length scale has increased.

We will now discuss the diffraction peaks arising from the mesopore lattice. Because of the hexagonal bundling of the long cylindrical pores, Bragg-like peaks appear prominently in the diffraction pattern of MCM-41 and the peaks can be indexed in terms of 2-dimensional Miller indices (*hk*). The strong peak at $Q = 0.164$ Å^{-1} is the first-order peak (10), while the broad and weaker peaks at ~0.28 Å^{-1} and ~0.33 Å^{-1} are the higher-order peaks (11) and (20), respectively (seen most clearly in the inset of Fig. 2). With increasing amount of pentane adsorbed, the (10) peak intensity was seen to increase by ~40% before decreasing almost to zero at the pressure $P/P^* = 0.28$ and above. In contrast, the higher order peaks do not show an initial increase: they monotonically decrease and seem to reach the background level well before the (10) peak does. We have enough counting statistics to be sure that the higher order peaks do not increase throughout the adsorption cycle, at least not by as much as 40% (see Fig. 3). The disappearance of (10) diffraction peak at $P/P^* \sim 0.28$ clearly coincides with the onset of the plateau in the adsorption isotherm (Fig. 4), identifying it as the complete filling of the mesopores. This also shows that the particular ratio we adopted for C_5H_{12}/C_5D_{12} mixing led to satisfactory contrast matching.

As intriguing as they may be, the results on Bragg peaks described above are not new. Complete quenching of diffraction peaks is usually taken as the evidence that all the pores contributing to the diffraction are accessible by the contrast-matched adsorbate. The initial increase of the first order Bragg peak is known not only for MCM-41 but also for other similar mesoporous materials (see the extensive review by Hoinkis [14]; specifically p. 90–91). Therefore, our results are not likely to cause surprise or controversy. The reason for the increase, however, may not be properly understood and could become a matter of debate as explained below.

In the year 2000, Tun and Mason [15] pointed out that the (10) peak intensity is extremely sensitive to the cylindrical pore diameter *D*. Their prediction is based on a model consisting of an ensemble of cylindrical pores. The diffraction intensity these authors calculated from the model is the square of the product of (*i*) the form factor of a long cylinder, $F_c(Q)$, and (*ii*) the structure factor of points representing the position of the cylinders, arranged fairly accurately on a hexagonal lattice locally but the positional error increasing linearly with distance from the origin. For a long cylinder of diameter *D* taken arbitrarily to be in the *z* direction, $F_c(Q)$ is related to the Bessel function $J_1\{(D/2)Q_{xy}\}$ as

$$F_c(Q) = (\pi\rho D/Q_{xy})\, J_1\{(D/2)Q_{xy}\}\delta(Q_z)$$

where ρ is the contrast at the pore walls, and the δ-function ensures only those pores with cylindrical axes perpendicular to $\boldsymbol{Q}$ contribute to scattering (i.e., observed intensity comes only from those powder grains that are oriented in a particular way). Consequently, we only need to consider the case where $Q = Q_{xy}$ and $Q_z = 0$. As our diffraction experiment and the analysis involve only intensities on an arbitrary scale, we shall set $\rho = 1$ for the contrast between the SiO_2 skeleton and the empty space within the pore.

Figure 5 is the plot of the cylindrical form factor square, $|F_c(Q)|^2$, for the pore diameters 36, 34, 32, and 30 Å, and the vertical lines mark the positions of the (10), (11), and (20) peaks for the inter-cylinder spacing of our sample (44.2 Å). The smaller cylinders mimic the reduction of the central empty space as the contrast-matched pentane coats the inside pore walls. The figure immediately suggests an explanation as to why the (10) peak increases in the initial phase of the adsorption process: although the overall spectral weight of the $|F_c(Q)|^2$ is lower for smaller cylinders (i.e., total area under the curve is less), its magnitude actually *increases* at the *Q* of (10). In contrast, for the higher order peaks, the magnitude decreases (for (11)) or does not change appreciably (for (20)).

Also in the year 2000, Ramsay et al. [16] reported an experimental observation of the increase of the first-order diffraction peak when contrast-matched benzene is adsorbed in SBA-15 silica. The mesoporous structure of SBA-15 is similar to MCM-41, except that its pores (and the inter-cylindrical distance) are much bigger. The authors tentatively ascribed the increase of (10) in early stage of adsorption to thickening of the effective pore walls. We note that the two groups of authors were considering exactly the same physical change: since the inter-cylindrical distance remains constant, reduction of pore diameter inevitably thickens the pore walls.

Another experimental observation of the increase of (10) peak during adsorption was reported a year later by Smarsly et al. [7] Two mesoporous silicas designated as SE1010 and SE3030 were investigated by in situ adsorption of nitrogen with SANS. Towards the end of adsorption, only a small trace of the mesoporous diffraction pattern remains, as there is accidental contrast matching between condensed nitrogen and the host material. Although the phenomenon overall is quite similar to the results by Ramsay et al. (and to ours as in Fig. 2), Smarsly et al. proposed a rather different explanation, namely that filling of micropores of the host material and smoothing of the walls by adsorbed nitrogen resulted in contrast enhancement between the host and the still empty pores. While this may be a valid explanation for SE1010 and SE3030, it is not consistent with the monotonic decrease of higher order peaks we observe for MCM-41. A higher contrast would make *all* peaks stronger, whereas in our case only the (10) peak shows the initial increase.

The above discussion raises an interesting question if the behaviour of the (10) peak is in anyway a universal phenomenon, i.e., one that can be expected for a certain class of materials on a general ground. For mesoporous materials with long cylindrical pores, the form factor will always be some form of a Bessel function. For the structure factor, the first-order peak will be quite sharp as long as the pores are of reasonably uniform size and do not intersect each other. This expectation is based on the fact that even for a fully disordered liquid, a hard sphere potential alone leads to a prominent first-order peak. A hard sphere potential prevents the centres of two particles to be closer than their diameter whereas, in our case, two non-intersecting pores cannot have centres closer than the sum of their radii. In Fig. 5, the first minimum of $|F_c(Q)|^2$ depends on the pore

diameter D (at $Q = 7.66/D$), while the (10) peak is given by the inter-cylindrical distance a (at $Q = 7.26/a$). For non-intersecting cylindrical pores, geometry requires $D < a$, but provided the intervening walls are not too thick the difference will be small. This places the (10) peak of the structure factor at a slightly smaller Q with respect to the first $|F_c(Q)|^2$ minimum. The (10) intensity will then increase upon a small reduction of effective pore diameter, and the phenomenon is simply a consequence of geometry.

The insight we now have for the changes in the diffraction pattern of MCM-41 provides us with a novel way of determining the cylindrical pore diameter. Figure 6 shows how the magnitude of the $|F_c(Q)|^2$ at $Q(10)$ will change as a function of the pore diameter. We see that at this particular Q, the intensity reaches a maximum at the pore diameter of $\sim$29 Å, corresponding to P/P^* of 0.16 (Fig. 2). Prior to this, including for the sample in vacuo, the (10) peak is weaker because the effective pore diameter is larger. Referring back to Fig. 2, the integrated intensity of the (10) peak above the $1/Q$ trend changes from 75 568 counts in vacuum to 120 102 counts representing a 59% increase. According to Fig. 6, the change is consistent with the empty pore diameter being 37 Å. Note that this result is based on intensities measured at a single point in Q-space. In contrast, we see in the literature diameter determinations based on intensities at two locations of Q [17, 18]. In terms of Fig. 5, the two-Q method amounts to comparing the intensities at two vertical lines and deciding which function gives the best fit. This approach will lead to an erroneous result for an obvious reason: the observed intensity variation with Q does not come entirely from the cylindrical form factor but also from the underlying structure factor. The latter is known only for an infinitely large ordered lattice. Electron micrographs of MCM-41 show large regions of good local order. However, being a two-dimensional ordering process with no constraints other than closed-packing of polymers, we do not expect the order to extend to infinity. The model proposed by Tun and Mason captures this essential feature, and as expected, gives a structure factor exhibiting Lorentzian-like peaks whose width increases with Q^2 (see Fig. 1 of ref. 15). Note that invoking Debye–Waller factors or finite-size ordered regions will not lead to a proper modeling of this diffraction pattern. The former will give a decrease of higher order peaks but without a broadening, while the latter will give *order-independent* broadening. It is therefore our opinion that analyses based on multiple points in Q (or worse based on the entire diffraction pattern) are all fundamentally flawed.

The 37 Å pore diameter is considerably larger than the 24 Å given by the BJH method, but the latter is known to underestimate the pore size [19]. It leads to a revised specific surface area of 809 m^2/g, and the total pore length 7.0×10^{10} m/g. The specific surface area thus obtained is still considerably smaller than the value based on the BET analysis (smaller by 30%). It is consistent with the view [20] that the N_2 BET method tends to overestimate surface area in siliceous materials. Apparently the same overestimation occurs for pentane since, as explained in the Experimental section, BET method yielded the same specific area for our sample with the two adsorbates.

We will finally comment on the $1/Q$ underlying trend of diffracted intensity. This component of scattering, seen as a straight line of slope –1 in a log–log plot (inset in Fig. 2), is the signature of scattering from a powder sample that contains phase-correlated regions within which the scattering-length density fluctuates in two orthogonal directions but remains constant in the third direction. Given that our sample is prepared from a template material that forms long parallel cylinders it is not surprising to have this component of scattering. Re-plotting all our data on the log–log plot shows that the $1/Q$ component exists at every pressure, increases and passes through a maximum as the pores in the MCM-41 are filled and reduces back approximately to the initial magnitude at the end of filling, i.e., it persists even when the pores are filled. Therefore, we conclude the $1/Q$ component does *not* originate from the pores themselves — if so, it would have been wiped out or greatly reduced when the pores are filled with a contrast-matched material. The $1/Q$ component is a measure of lateral (i.e., perpendicular to the cylindrical axis of the pores) correlations that are beyond the mesopore structure. They may be features caused by imperfect hexagonal packing or by inaccessible pores that are randomly distributed throughout the lattice. We cannot speculate much further except to recognize that these are the correlations not affected by the presence of pentane for 8 days, nor by traversing the adsorption–desorption cycle once.

4. Conclusions

Adsorption of pentane in a porous MCM-41 silica takes place without hysteresis in either the adsorption–desorption isotherm or the neutron scattering profile. The adsorption of contrast-matched pentane ultimately reduces the intensity of the Bragg peaks in the neutron scattering profile to zero. However, the intensity of the (10) peak initially increases in the early part of adsorption and in the late part of desorption. Identifying the origin of this behaviour as the coating the inside wall of the pores with contrast-matched pentane, we estimate the diameter of the empty pores as 37 Å.

Acknowledgements

This work is supported by the Natural Sciences and Engineering Research Council of Canada. RJCB and MJBE wish to acknowledge kind hospitality at Chalk River. ZT has benefited from discussions with Steve Spooner of Oak Ridge National Laboratories.

References

1. F. Rouquérol, J. Rouquérol, and K.S.W. Sing. Adsorption by powders and porous solids. Academic Press, London, UK. 1999.
2. G.C. Wall and R.J.C. Brown. J. Colloid Interface Sci. **82**, 141 (1981). doi:10.1016/0021-9797(81)90132-6.
3. G.J. Mason. J. Colloid Interface Sci. **88**, 36 (1982). doi:10.1016/0021-9797(82)90153-9.
4. J.D.F. Ramsay and G. Wing. J. Colloid Interface Sci. **141**, 475 (1991). doi:10.1016/0021-9797(91)90345-9.
5. J.D. Ramsay. *In* Handbook of porous solids. Vol. 1. 2002. pp. 135–235.
6. E. Hoinkis. Langmuir, **12**, 4299 (1996). doi:10.1021/la9600412.

7. B. Smarsly, C. Göltner, M. Antonietti, W. Ruland, and E. Hoinkis. J. Phys. Chem. B, **105**, 831 (2001). doi:10.1021/jp003105x.
8. S. Kallus, A. Hahn, and J.D.F. Ramsay. Eur. Phys. J. E, **12**, 31 (2003). doi:10.1140/epjed/e2003-01-008-2.
9. J.S. Beck, J.C. Vartuli, W.J. Roth, M.E. Leonowicz, C.T. Kresge, K.D. Schmitt, C.T.-W. Chu, D.H. Olson, E.W. Sheppard, S.B. McCullen, J.B. Higgins, and J.L. Schlenker. J. Am. Chem. Soc. **114**, 10834 (1992). doi:10.1021/ja00053a020.
10. R. Ryoo and J.M. Kim. Chem. Commun. 711 (1995). doi:doi:10.1039/C39950000711.
11. E.P. Barrett, L.G. Joyner, and P.P. Halenda. J. Am. Chem. Soc. **73**, 373 (1951). doi:10.1021/ja01145a126.
12. Z. Tun, P.C. Mason, F.K. Mansour, and H. Peemoeller. Langmuir, **18**, 975 (2002). doi:10.1021/la0014252.
13. Ch. Hörner, A. Höpfner, and B. Schmeiser. Ber. Bunsen-Ges. **79**, 222 (1975).
14. E. Hoinkis. Part. Part. Syst. Char. **21**, 80 (2004). doi:10.1002/ppsc.200400927.
15. Z. Tun and P.C. Mason. Acta Crystallogr. A, **56**, 536 (2000). doi:10.1107/S0108767300009740. PMID:11058839.
16. J.D.F. Ramsay, S. Kallus, and E. Hoinkis. Stud. Surf. Sci. Catal. **128**, 439 (2000). doi:10.1016/S0167-2991(00)80049-X.
17. M. Impéror-Clerc, P. Davidson, and A. Davidson. J. Am. Chem. Soc. **122**, 11925 (2000). doi:10.1021/ja002245h.
18. P.-A. Albouy and A. Ayral. Chem. Mater. **14**, 3391 (2002). doi:10.1021/cm0211453.
19. P.I. Ravikovitch, D. Wei, W.T. Chueh, G.L. Haller, and A.V. Neimark. J. Phys. Chem. B, **101**, 3671 (1997). doi:10.1021/jp9625321.
20. M. Kruk, M. Jaroniec, and A. Sayari. Langmuir, **13**, 6267 (1997). doi:10.1021/la970776m.

List of symbols

a	spacing between the centres of cylindrical pores
D	diameter of cylindrical pores
$F_c(Q)$	form factor of cylinder
(hk)	Miller indices
$J_1(\ldots)$	Bessel function of the first kind
P	pressure or vapour pressure
P^*	vapour pressure at sample temperature
$\boldsymbol{Q}$	scattering vector
Q	magnitude of scattering vector
Q_{xy}	component of scattering vector in xy-plane
Q_z	component of scattering vector along z-axis
T	temperature
$\delta(\ldots)$	delta function
ρ	contrast